

HI 21cm probes of reionization, and beyond

C.L. Carilli¹

¹*National Radio Astronomy Observatory, Socorro, NM, USA, 87801*

E-mail: ccarilli@nrao.edu

Abstract

I review the potential for observing cosmic reionization using the HI 21cm line of neutral hydrogen. Studies include observations of the evolution of large scale structure of the IGM (density, excitation temperature, and neutral fraction), through HI 21cm emission, as well as observations of small to intermediate scale structure through absorption toward the first discrete radio sources. I summarize predictions for the HI signals, then consider capabilities of facilities being built, or planned, to detect these signals. I also discuss the significant observational challenges.

Key words: cosmology, radio, lines

1 Introduction

The 21cm line of neutral hydrogen presents a unique probe of the evolution of the neutral intergalactic medium (IGM), and cosmic reionization. Furlanetto & Briggs (22) point out some of the advantages of using the HI line in this regard: (i) unlike $\text{Ly}\alpha$ (ie. the Gunn-Peterson effect), the 21cm line does not saturate, and the IGM remains 'translucent' at large neutral fractions (12). And (ii) unlike CMB polarization studies, the HI line provides full three dimensional (3D) information on the evolution of cosmic structure, and the technique involves imaging the neutral IGM directly, and hence can easily discern different reionization models (3; 25). HI 21cm observations can be used to study evolution of cosmic structure from the linear regime at high redshift (ie. density-only evolution), through the non-linear, 'messy astrophysics' regime associated with luminous source formation. As such, HI measurements are sensitive to structures ranging from very large scales down to the source scale set by the cosmological Jeans mass, thereby "making 21cm the richest of all cosmological data sets" (3).

Early calculations of HI 21cm signal from a neutral IGM discuss a broad range of models for large scale HI structure, including Zeldovich 'pancakes' arising

in HDM models, explosive structure formation models, and CDM (64; 34; 58). Early (unsuccessful) searches for large scale structure in HI based on this wide range of predictions include searches for pancakes with masses $> 10^{14} M_{\odot}$ at $z \sim 3$ (66; 53; 18; 19), and for even more massive structures ($10^{15} M_{\odot}$) at $z = 8.4$ (5). Fortunately, the cosmological parameter space has been greatly reduced due to the advent of the concordance model of Λ CDM structure formation, and this paper will assume the standard precision cosmology parameters (62).

In this review I will summarize the HI 21cm probes of cosmic reionization and the neutral IGM. I will focus on the latest predictions for the expected signals, and the observational capabilities of telescopes being built, or planned, to detect these signals. I begin with a short basic review of the physical processes involved in reionization that relate directly to the HI 21cm signal. Previous reviews that dealt with, at least in part, the HI 21cm signal from cosmic reionization, include (4; 41; 44), and in the context of the Square Kilometer Array (SKA) (10; 22). See also articles by Furlanetto, Morales, and Peterson in this volume.

2 The physics of the neutral IGM

The physics and equations of radiative transfer of the HI 21cm line through the neutral IGM have been considered in detail by many authors (58; 6; 22; 77; 57; 65; 43; 48), and I review only the basic results here.

In analogy to the Gunn-Peterson effect for $\text{Ly}\alpha$ absorption by the neutral IGM, the optical depth, τ , of the neutral hydrogen to 21cm absorption for our adopted values of the cosmological parameters is:

$$\tau = \frac{3c^3 h_p A_{10} n_{HI}}{32\pi k_B \nu_{21}^2 T_S H(z)} \sim 0.0074 \frac{x_{HI}}{T_S} (1 + \delta)(1 + z)^{3/2}, \quad (1)$$

This equation shows immediately the rich physics involved in studying the HI 21cm line during reionization, with τ depending on the evolution of cosmic over-densities, δ (predominantly in the linear regime), the neutral fraction, x_{HI} (ie. reionization), and the HI excitation, or spin, temperature, T_S .

In the Raleigh-Jeans limit, the observed brightness temperature (relative to the CMB) due to the HI 21cm line at a frequency $\nu = \nu_0/(1 + z)$, where $\nu_0 = 1420.40575$ MHz, is given by:

$$T_B \approx \frac{T_S - T_{CMB}}{1 + z} \tau \approx 7(1 + \delta)x_{HI}\left(1 - \frac{T_{CMB}}{T_S}\right)(1 + z)^{1/2} \text{ mK}, \quad (2)$$

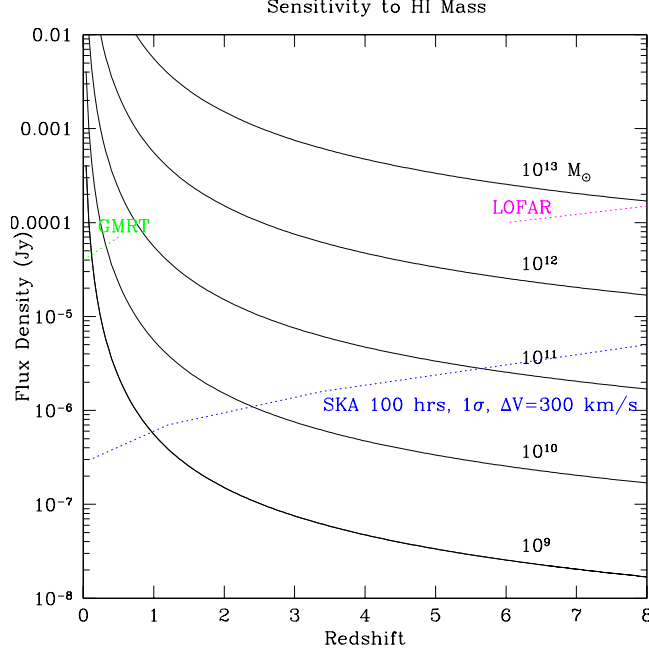


Fig. 1. The HI mass sensitivity versus redshift in 100hrs, for 300 km s⁻¹ line width.

The conversion factor from brightness temperature to specific intensity, I_ν , is given by: $I_\nu = \frac{2k_B}{(\lambda_{21}(1+z))^2} T_B$, or in more common units: $I_\nu = 7.1 \times 10^4 (1+z)^{-2} T_B$ Jy sr⁻¹. Equation 2 shows that for $T_S \sim T_{CMB}$ one expects no 21cm signal. When $T_S \gg T_{CMB}$, the brightness temperature becomes independent of spin temperature. When $T_S \ll T_{CMB}$, we expect a strong negative (ie. absorption) signal against the CMB.

An important point to keep in mind is that, for the 21cm experiments being considered, the signal being observed corresponds to large scale structure, not individual galaxies. This point is demonstrated in Fig 1, which shows the expected signal in Jy versus redshift for different HI masses, along with the expected sensitivity of current and future radio telescopes. For simplicity, I have assumed a single line width of 300 km s⁻¹, which would correspond to individual virialized galaxies, or to large scale structures just separating from the Hubble flow. Fig 1 shows that current instruments, such as the GMRT, can detect large galaxies ($\sim 10^{10} M_\odot$ in gas) out to only modest redshifts ($z \leq 0.3$), even in long integration times. At redshifts corresponding to reionization ($z > 6$), future large area low frequency radio telescopes, such as LOFAR, and eventually the SKA, will still be limited to studying large scale structure (HI masses $> 10^{11}$ to $10^{12} M_\odot$). Fortunately, the entire IGM is made up of neutral hydrogen prior to reionization, and the large scale structure detected is not just density enhancements (ie. protoclusters), but also structure induced by reionization itself (the 'bubble machine' of HII regions), and possibly spatial variations in the spin temperature.

(65) show that the HI excitation temperature will equilibrate with the CMB on a timescale $\sim \frac{3 \times 10^5}{(1+z)}$ year, in absence of other effects. However, collisions and resonant scattering of Ly α photons can drive T_S to the gas kinetic temperature, T_K (21; 70):

$$T_S = \frac{T_{\text{CMB}} + y_c T_K + y_{\text{Ly}\alpha} T_K}{1 + y_c + y_{\text{Ly}\alpha}}. \quad (3)$$

In this equation, y_c represents collisional excitation of the hyperfine transition, which couples T_S to the gas kinetic temperature T_K . The coupling coefficient $y_c \propto n_H$, and (79) shows that, for the mean IGM density, collisional coupling between T_S and T_K becomes significant for $z \geq 30$. The third term in equ 3 corresponds to the Wouthuysen-Field effect, in which resonant scattering of Ly α photons couples the spin temperature to T_K (70; 21; 8; 33; 43; 44; 55). (43) show that this latter mechanism will be important when the radiation background at the Ly α frequency satisfies $J_\alpha > 9 \times 10^{-23} (1+z) \text{ erg cm}^{-2} \text{ s}^{-1} \text{ Hz}^{-1} \text{ sr}^{-1}$, or about one Ly α photon per every two baryons at $z = 8$ (8).

The interplay between the CMB temperature, the kinetic temperature, and the spin temperature, coupled with radiative transfer, lead to a number of interesting physical regimes for the HI 21cm signal. (1; 3) suggest the following plausible regimes:

At $z > 200$ residual free electrons couple T_{CMB} and T_K through Thompson scattering and subsequent gas collisions, while the density is high enough to equilibrate T_K and T_S . In this case $T_S = T_{\text{CMB}}$ and there is no 21cm signal.

At $z \sim 30$ to 200, the residual ionization fraction and density is too low to couple T_K to T_{CMB} , so the gas cools adiabatically, with temperature falling as $(1+z)^2$, ie. faster than the $(1+z)$ for the CMB. Hence the gas becomes colder than the CMB. However, the mean density in this redshift range is still high enough to provide some coupling between T_S and T_K through collisions, and the HI 21cm signal might be seen in absorption against the CMB. In this regime the HI fluctuations are still evolving linearly, essentially following the dark matter (3; 42; 59).

At $z \sim 20$ to 30, the situation starts to become complex. Collisions can no longer couple T_K to T_S , and T_S again approaches T_{CMB} . However, we might also expect the first luminous structures (Pop III stars or mini-quasars), at least near the end of this redshift range. The Ly α photons from these objects would induce local coupling of T_K and T_S , thereby leading to some 21cm absorption regions. On the other hand, (3; 43) point out that these same photons, and more importantly, any Xrays from the first luminous sources (14), could lead to local IGM warming above T_{CMB} well before reionization. Energetically it takes 13.6 eV per baryon to ionize the IGM, but only $0.005 \frac{(1+z)}{20}$

eV to warm the IGM about T_{CMB} . Hence one might expect a 'patch work' of regions with no signal, absorption, and perhaps emission, in the 21cm line.

At $z \sim 6$ to 20 all the physical processes come to play. The IGM is being warmed by the resonant scattering of Ly α photons (43), and penetrating, ionizing hard Xrays, from the first galaxies and black holes (42; 3; 8), as well as by weak shocks associated with structure formation (25; 27; 57; 14), such that T_K is likely larger than T_{CMB} globally (25). Likewise, these objects are reionizing the universe, leading to a fundamental topological change in the IGM, from the linear evolution of large scale structure, to a bubble dominated era of HII regions (26). It is this regime that most (although not all), theoretical work has been exploring, and the expected HI 21cm signal is rich. Finally, after reionization, $z < 6$ to 10, the IGM is fully ionized ($x_{HI} < 10^{-4}$), and the 21cm signal is gone.

3 HI 21cm probes of the evolution of the IGM

3.1 Global HI signature

In an idealized sense, if the universe reionized very rapidly everywhere, at the same time, one would expect a global (ie. full sky) step in the background temperature at the frequency corresponding to the redshifted 21cm line (60). However, if nothing else, cosmic variance will lead to different ionization redshifts in different regions, and we now know that reionization is likely an extended process in time, thereby smoothing out the expected signal in space and time. On the other hand, since this is an all sky signal, the sensitivity of the experiment is independent of telescope collecting area, and the experiment can be done using small area telescopes at low frequency, with well controlled frequency response.

The most recent modeling of the expected global HI signal is presented in (27) (see also (25)), who employ the numerical simulations of (29). They include both a fast reionization model, plus more complicated, *ad hoc* reionization histories.

Results from these calculations are reproduced in Fig 2a. The expected signal peaks at roughly 20 mK above the foreground. In their fiducial (fast reionization) model, the peak occurs at $z \sim 10$. They also predict a negative signal, meaning absorption against the CMB, at higher redshift, prior to IGM warming, but allowing for Ly α resonant scattering (ie. the era of 'Ly α coupling' (3)). The shaded region shows the potential system thermal noise of a well calibrated low frequency experiment.

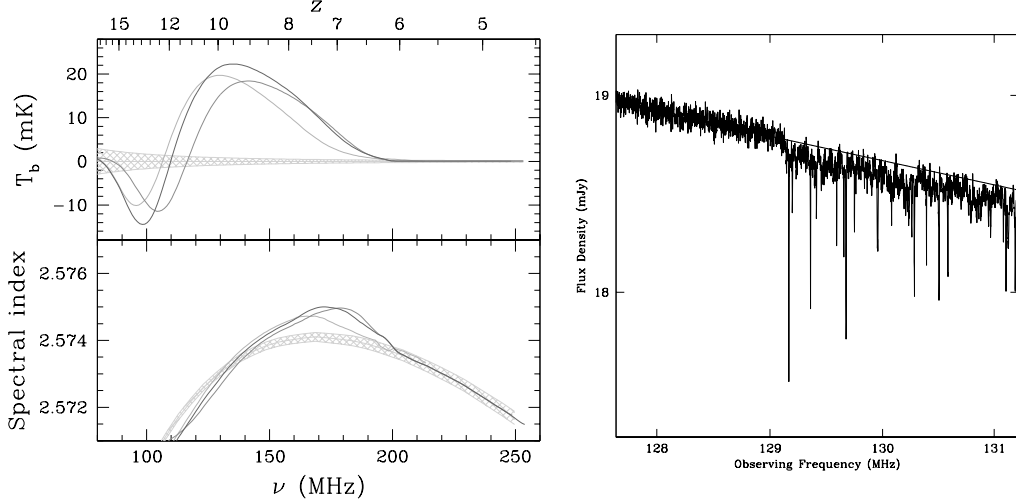


Fig. 2. Left: Global (all sky) HI signal from reionization (27). The shaded region shows the expected thermal noise in a carefully controlled experiment. Right: The simulated spectrum of a source with $S_{120} = 20$ mJy at $z = 10$ using a spectral model based on the powerful radio galaxy Cygnus A and assuming HI 21cm absorption by the IGM (12). Thermal noise has been added using the specifications of the SKA and assuming 10 days integration with 1 kHz wide spectral channels. The onset of absorption by the neutral IGM is seen at 129 MHz, corresponding to the HI 21cm line at $z = 10$.

(27) point out that detecting this signal against the mean non-thermal foreground radiation may be difficult. The foreground is the sum of relatively smooth Galactic synchrotron emission and discrete distant radio galaxies, with a typical spectral index, $\alpha \sim -0.8$, where α is defined as: $S_\nu \propto \nu^\alpha$. The foreground temperature behaves roughly as $T_{FG} \sim 100(\frac{\nu}{200\text{MHz}})^{-2.8}$, in the coldest regions of the sky, and can be an order of magnitude higher in the Galactic plane. Hence, the expected change in T_B is at most $\sim 10^{-4}$ that of the mean foreground signal over the frequency range ~ 100 to 200 MHz.

3.2 Large scale structure

3.2.1 Power spectra and tomography

The majority of theoretical studies have focused on predicting the HI fluctuations in the IGM on scales of arcmins to a few degrees both during (78; 43; 65; 24; 25; 3; 1; 6; 27; 57; 26; 68), and prior to (8; 2; 42), reionization. Most studies have focused on the diffuse IGM, although a few studies have also considered the signal expected due to the clustering of collapsed structures (36).

The HI 21cm signal from the IGM during reionization can be predicted both analytically, using a standard Press-Schechter type of analysis of linear struc-

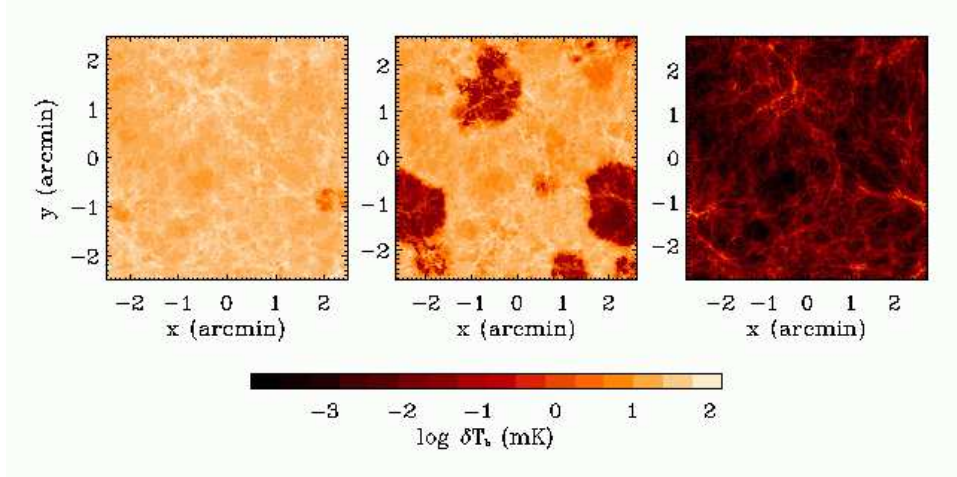


Fig. 3. The simulated HI 21cm brightness distribution during reionization at $z = 12$, 9, 7 (76; 24).

ture formation, plus some recipes to approximate non-linear evolution (57; 76; 1; 6; 27), or through the use of numerical simulations (8; 25).

Fig 3 shows the expected evolution of the HI 21cm signal during reionization based on the numerical simulations of (25). They find that the mean HI signal is about $T_B \sim 25$ mK prior to reionization, with fluctuations of only a few mK on arcmin scales due to linear density evolution. In this simulation, the HII regions caused by galaxy formation during reionization are seen in the redshift range $z \sim 8$ to 10, reaching scales up to $2'$ (frequency widths ~ 0.3 MHz $\Rightarrow 0.5$ Mpc physical size). These regions have (negative) brightness temperatures up to 20 mK relative to the mean HI signal. This corresponds to $5\mu\text{Jy beam}^{-1}$ in a $2'$ beam at 140 MHz.

We compare this signal to the sensitivity of a radio array. The point source rms sensitivity (dual polarization) in an image from a synthesis radio telescope is given by:

$$\text{rms} = \left(\frac{70}{(\Delta\nu_{\text{kHz}} t_{\text{hr}})^{0.5}} \right) \left(\frac{T_{\text{sys}}}{300\text{K}} \right) \left(\frac{0.60}{\epsilon_{\text{eff}}} \right) \left(\frac{500\text{m}^2}{A_{\text{ant}}} \right) \left(\frac{27}{N_{\text{ant}}} \right) \text{ mJy beam}^{-1} \quad (4)$$

where $\Delta\nu$ is the channel width in kHz, t is the integration time in hours, T_{sys} is the total system temperature, A is the collecting area of each element in the array, ϵ is the aperture efficiency, and N is the number of elements (ϵAN = total effective collecting area of the array). At low frequency the value of T_{sys} is dominated by the non-thermal foreground, and again behaves as $T_{\text{sys}} \sim 100 \left(\frac{\nu}{200\text{MHz}} \right)^{-2.8}$ K. The beam FWHM is given by the Fourier transform of the uv coverage, assuming equal weight for each visibility.

Consider an array with an effective collecting area of 1 square kilometer at 140

MHz, distributed over 4 km, a system temperature of 300 K, a channel width of 0.3 MHz, and integrating for one month. The rms sensitivity is then $1.3\mu\text{Jy beam}^{-1}$, with a beam FWHM $\sim 2'$. This square kilometer array will be just adequate to perform true three dimensional imaging of the average structure of the IGM during reionization.

Unfortunately, the nearer term low frequency 'path finder' arrays will have $\leq 10\%$ the collecting of the SKA, and will likely not be able to perform such direct 3D imaging (Table 1). However, these near term experiments should have enough sensitivity to perform power spectral analyses of the HI 21cm fluctuations. For power spectral analyses the sensitivity is greatly enhanced relative to direct imaging due to the fact that the universe is isotropic, and hence one can average the measurements in annuli in the uv-plane, ie. the statistics of fluctuations along a uv annulus are equivalent. The width of independent uv annuli is set by the primary beam diameter, D, or $\Delta l = 2\pi \frac{D}{\lambda_{obs}}$. The situation is analogous to COBE and WMAP. COBE lacked the sensitivity to make a true image of the CMB fluctuations, but was able to make a robust determination of the power spectrum of fluctuations. WMAP was able to produce a proper image of the CMB.

Many authors have considered the power spectrum of brightness temperature fluctuations in the HI 21cm line (57; 76; 1; 6; 48; 63; 7). It can be shown that the noise power spectrum, in mK^2 , in standard spherical harmonic units, $\frac{l(l+1)}{2\pi} C_l^N$, for an array with uniform coverage of the uv plane, is given by:

$$C_l^N = \frac{T_{sys}^2 (2\pi)^3}{\Delta\nu t f_c^2 l_{max}^2} \quad (5)$$

where f_c = areal covering factor of the array = $N_{ant} \frac{A_{ant}}{A_{tot}}$, and A_{tot} is the total area of the area defined by the longest baseline. For example, for the logarithmic antenna spacing of the VLA in the smallest configuration, the VLA-VHF system has $f_c = 0.017$ on baselines out to 1 km, and $f_c = 0.17$ out to 0.25 km, for a full synthesis observation. For comparison, the SKA will have 30% of it's collecting area inside 1 km, or $f_c = 0.3$ out to 1 km.

Most predictions of the HI 21cm power spectrum during reionization published thus far parallel the 2D calculations applied to the CMB. Ultimately, higher sensitivity, and physical insight, will come through full 3D analysis of the HI 21cm fluctuations during reionization (48). Of course, at the smallest l , approaching the primary beam size Δl , the signal-to-noise is limited by cosmic variance to essentially the number of synthesized beams per primary beam.

As an example, Fig 4 shows the predicted evolution of the HI 21cm power spectrum using an analytic calculation of structure formation, including a model of (uncorrelated) HII region formation during reionization (25; 76) (see

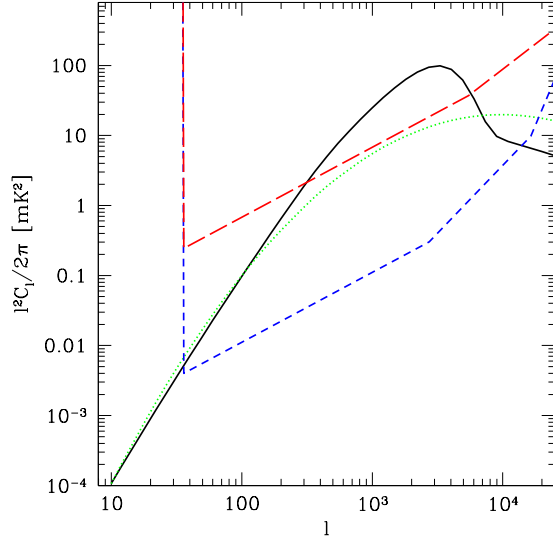


Fig. 4. Predicted HI 21cm brightness temperature power spectrum during reionization at $z = 10$ (22; 76). The green dotted line is the model prediction including only linear density fluctuations. The black line solid includes the effect of HII regions during reionization. The red long dash line shows the sensitivity of pathfinder experiments like LOFAR, while the blue short dash curve shows the sensitivity for the SKA, assuming $\log l$ bins. The cutoff at low l is set by the primary beam.

also (6; 57; 68) for analytic solutions, and (25; 8) for predictions based on numerical simulations). Fig 4 includes the power spectrum arising from linear density fluctuations following the dark matter, plus the effect of reionization. The signature of reionization can be seen as a bump in the power spectrum above the density-only curve due to the formation of HII regions. In this calculation, the rms fluctuations at $z = 10$ peak at about 10 mK rms (observing frequency = 130 MHz) on scales $l \sim 3000$ ¹. Note that in this calculation the neutral fraction as a function of redshift is a free parameter, and is assumed to be 0.5 at $z = 10$. (3) point out that there is no very large scale information contained in the HI 21cm fluctuations, and that power spectral analyses are best done on scales ranging from $l = 100$ to a few thousand, ie. on angular scales \leq few degrees.

Also included are the noise power spectra for near and longer term radio arrays. Typical noise values for near-term arrays are ~ 1 to 10 mK rms in the range $l = 10^3$ to 10^4 , for long integrations. This should be adequate to determine the HI 21cm power spectrum during reionization. The SKA will go an order of magnitude deeper, providing an accurate measure of the HI power spectrum, and its evolution with redshift.

¹ or $u = \frac{l}{2\pi} = 500$, or $\theta \sim \frac{180^\circ}{l} = 3.6'$, or baselines, $b = \lambda u = 1.2$ km, or wavenumber $k \sim \frac{l}{10^4} \text{Mpc}^{-1} = 0.3 \text{Mpc}^{-1}$ (comoving).

(2; 1) have shown that gas peculiar velocities, ie. infall into superclusters and along filaments (analogous to the Kaiser effect for galaxy clustering), increases the expected rms fluctuations by about a factor two. Also, clustering of luminous sources (ie. biased galaxy formation) implies a characteristic scale for the HII regions of 1 to 10 Mpc (comoving), and leads to another factor two in fluctuation strength (26; 57) over the random distribution of HII regions assumed by (77). Specifically, this later effect moves the fluctuation power to larger scales.

(77; 6; 25) consider the effect of spectral channel width on the power spectral analysis. Bandwidth enters via the finite thickness of the HII regions and the density fluctuations. They conclude that a bandwidth of about 0.2 MHz is optimal for power spectral studies, although the rms of the signal changes by only a factor of about two going from 0.1 to 0.5 MHz channel width.

(25) show how the power spectra change with different reionization models, including outside-in versus inside-out models, uniform versus HII region dominated reionization, and double reionization. They point out that HI 21cm power spectral studies should provide powerful constraints on the process of reionization, with different reionization scenarios clearly discernable in their power spectral signature. Note that this is unlike CMB large scale polarization measurements, which provide reasonable constraints on the total Thompson scattering optical depth through the universe back to recombination, but only marginal constraints on the reionization history (35).

Lastly, (6; 49) point out that if full 3D tomography of the evolution of IGM structures could be made, then one might also constrain the geometry of universe through the standard Alcock-Pacinsky effect, ie. the difference in structure evolution observed in angle versus along the line-of-sight, due to the non-Euclidean geometry of the universe.

3.2.2 *Clustering of minihalos*

A point of debate has been the fraction of HI in collapsed objects, as opposed to the diffuse IGM (36). This fraction has a complex dependence on structure formation history, and (52; 28) conclude that the majority of the HI during reionization will remain in the diffuse phase. However, at times when T_S approaches T_{CMB} in the diffuse IGM, one might expect HI 21cm emission due to clustering of minihalos², in which $T_S > T_{CMB}$ simply due to the virialization

² Minihalos have masses $< 10^7 M_\odot$, and virial temperatures $< 10^4$ K. These halos cannot cool via atomic hydrogen lines, and therefore 'saturate' at over-densities of $\delta \sim 100$. They will not form stars unless an alternate cooling mechanism can be found. One candidate is molecular hydrogen, which is an effective coolant down to virial temperatures of 100 K (4).

process (25).

(36) have considered the HI 21cm power spectrum due to clustering of minihalos at high redshift. For a beam size of $1'$, and channel width of 0.2 MHz, they predict 3σ brightness temperature fluctuations due to clustering of minihalos $\sim 7\text{mK}$ at $z = 8.5$, decreasing to 2mK at $z = 20$.

3.2.3 Other tests

(16) discuss circular polarization of the 21cm line due to zeeman splitting during reionization. Such polarization would be detectable with the SKA if the IGM field strength were $100 \mu\text{G}$. (56; 15) consider the anti-correlation between HI 21cm fluctuations and sub-degree scale CMB secondary anisotropies due to Thompson scattering in ionized regions during reionization at $l > 1000$ (kinetic SZ effect). A natural anticorrelation would be expected between the neutral and ionized regions. And lastly, (61) discuss delensing of the CMB using the HI 21cm fluctuations to pin-point density inhomogeneities along the line of sight ($z \sim 10$ to 200). This could prove important for decoupling the E and B mode mixing that occurs due to lensing, possibly recovering the intrinsic (inflationary) B polarization.

3.2.4 Cosmic Stromgren spheres

While direct detection of the typical structure of HI and HII regions may be out of reach of the near-term 21cm telescopes, there is a chance that even this first generation of telescopes will be able to detect the rare, very large scale HII regions associated with luminous quasars near the end of reionization.

The presence of cosmic Stromgren spheres around the highest redshift SDSS QSOs has been deduced from the observed difference between the redshift of the onset of the GP effect and the systemic redshift of the host galaxy (69; 72; 71; 67) (although cf. (50)). The physical size of these spheres is ~ 5 Mpc, or an order of magnitude larger than the typical spheres expected from clustered galaxy formation, due to the extreme luminosity of the sources ($\sim 10^{14} L_{\odot}$). If the neutral fraction remains substantial to relatively low redshift, $f(\text{HI}) > 0.1$ (46; 72; 71), then it is plausible to search for these regions as 'holes in the sky', or regions of negative brightness in the redshift 21cm line frequency. The expected signal is $\sim 20\text{mK} \times f(\text{HI})$ on a scale $\sim 10'$ to $15'$, with a line width of ~ 1 to 2 MHz (73). This corresponds to $0.5 \times f(\text{HI})$ mJy beam^{-1} , for a $15'$ beam.

Searching for HI signals around known high redshift QSOs has a number of major observational advantages: (i) the exact location in frequency, and RA and DEC, are well determined, thereby limiting the search space dramatically, and

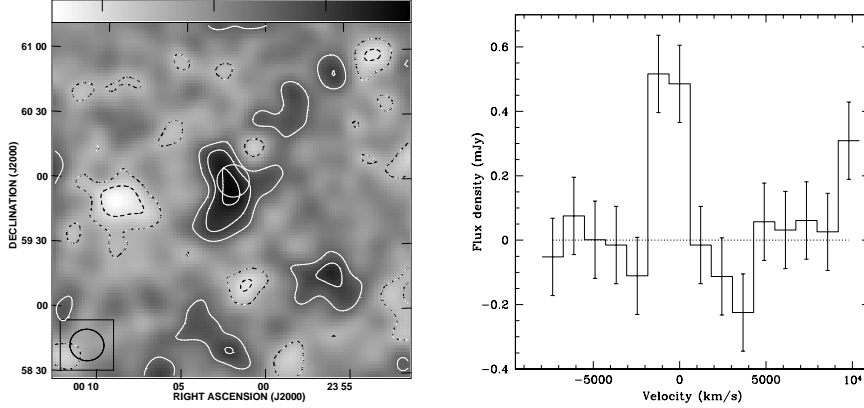


Fig. 5. Simulated image and spectrum of a Stromgren sphere surrounding a luminous SDSS QSO at the end of reionization for a 250 hour integration with the VLA-VHF system (86). The contour levels are: -0.45, -0.3, -0.15, 0.15, 0.3, 0.45 mJy beam⁻¹, and the negative signal has been inverted to appear positive.

(ii) there is already evidence for the existence of the features based on the Ly α spectra. The VLA-VHF system has been specifically design to search for these spheres around known SDSS quasars at $z \sim 6$ to 6.4 (86). Fig 5 shows the simulated image and spectrum of such a Stromgren sphere around an SDSS QSO assuming $f(\text{HI}) = 1$, as observed with the VLA-VHF system. While it is unlikely the mean neutral fraction is this high at such a low redshift, in 250 hours the VLA-VHF system should set the first direct constraints on neutral fraction of the IGM, at the level $f(\text{HI}) \geq 0.2$, as well as easily rule out more extreme models, such as $T_S \ll T_{\text{CMB}}$. (74) present similar simulations for the MWA and the SKA.

(39) also discuss spectral dips due to large HII regions around luminous quasars ($> 2 \times 10^{10} L_{\odot}$) during the EoR. Their Fig 2 shows a spectrum in a typical 10' beam from 100 to 180 MHz. They predict on average one relatively deep (-2 to -4 mK) dip per LoS on this scale. They emphasize that these spectral features may be easier to detect than spatial fluctuations of a similar magnitude, due to the fact that spatial confusion is highly structured on arcsec to arcmin scales, while the spectral confusion should be smooth over 10's of MHz.

(74) perform a similar calculation using the evolution of the bright QSO luminosity function to predict the number of HII regions around active QSOs at $z > 6$. They conclude that there should be roughly one SDSS-type HII region around an active QSO (physical radius $> 4\text{Mpc}$) per 400 deg² field per 16 Mhz bandwidth at $z \sim 6$, and one $R \geq 2\text{Mpc}$ region at $z \sim 8$. They also point out that the recombination time may be longer than the Hubble time, so that fossil HII regions may be observed around non-active AGN. Assuming a duty cycle $\sim \frac{\langle t_{\text{qso}} \rangle}{t_H(z)} \sim \frac{10^7}{10^9} \sim 0.01$, where $\langle t_{\text{qso}} \rangle$ is the fiducial lifetime of QSO

activity (75), and $t_H(z)$ is the age of the universe, leads to a factor 100 more fossil HII regions per FoV.

3.2.5 *Beyond reionization*

A number of authors have considered the brightness temperature fluctuations due to the 21cm line from the neutral IGM at redshifts prior to reionization, $z > 20$. (3; 2) predict the power spectrum of fluctuations during the era when the Ly α photons from the first luminous objects couple T_S to T_K locally, but the universe remains substantially neutral ($z \sim 20$ to 30), and $T_K < T_{CMB}$ in the diffuse IGM. Brightness temperature fluctuations can be due to emission from clustered minihalos, plus enhanced by absorption against the CMB by the diffuse IGM, with an rms ~ 10 mK for $l \sim 10^5$, due to a combination of linear density fluctuations, plus poisson ('shot') noise and biasing in the Ly α source (ie. galaxy) distribution.

(42) go even further in redshift, to $z > 50$ to 200. In this regime the HI generally follows linear density fluctuations, and hence the experiments are as 'clean' as CMB studies, and $T_K < T_{CMB}$, so a relatively strong absorption signal might be expected. (42) also point out that Silk damping, or photon diffusion, erases structures on scales $l > 2000$ in the CMB at recombination, corresponding to comoving scales = 22 Mpc. The HI 21cm measurements can explore this physical regime at $z \sim 50$ to 300. The predicted rms fluctuations are 1 to 10 mK on scales $l = 10^3$ to 10^6 (0.2° to $1''$). These authors point out that, due to sensitivity to large l , and the 3D nature of the information, HI 21cm power spectral studies in this epoch "contain an amount of information orders of magnitude larger than any other cosmological probe". These data could provide the best tests of non-Gaussianity of density fluctuations, and for constraining the tilt, or running power law index, of mass fluctuations to large l , providing important tests of inflationary structure formation. (59) also suggests that a large global signal, up to -0.1 K, might be expected for this redshift range.

Two experiments are being planned to cover this low frequency range, the long wavelength array (LWA) in New Mexico, and in the longer term, LUDAR is being considered for the back side of the moon.

3.3 *Absorption toward discrete radio sources*

Observing HI 21cm emission from the EoR implies studying large scale structure (cluster scales and larger). A number of groups have recently considered the possibility of studying smaller scale structure in the neutral IGM by looking for HI 21cm absorption toward the first radio-loud objects (AGN, star

forming galaxies, GRBs) (10).

(12) use numerical simulations to predict the HI 21cm absorption profile of the 'cosmic web' prior to reionization. For example, for a source at $z = 10$, they predict an average optical depth due to 21cm absorption of about 1%, corresponding to the 'radio Gunn-Peterson effect'. They also find about five narrow (few km/s) absorption lines per MHz with optical depths of a few to 10% (Fig 2b). These latter lines are equivalent to the Ly α forest seen after reionization, and correspond to over-densities evolving in the linear regime ($\delta \leq 10$). While significant questions remain about simulating the thermal state of the IGM to such detail, the simple point remains that, while the Ly α lines from such structures are highly saturated, the (much) lower 21cm oscillator strength makes the IGM translucent prior to reionization.

(23; 51) predict a similar HI 21cm absorption line density due to gas in minihalos as that expected for the 21cm forest. (13) shows that the presence or absence of HI absorption by minihalos, or the cosmic web, would be a telling diagnostic of early IGM heating mechanisms. (23) also consider the expected 21cm absorption profiles for proto-disk galaxies. While such absorption lines will be rare (10^4 times less frequent than the 21cm forest lines), the optical depths may be large enough that the lines could be observed toward faint radio sources, in particular, gamma ray burst radio after-glows within the host galaxy (37).

An important caveat in these calculations is the assumption of radio loud sources during the EoR. This question has been considered in detail by (12; 30; 38). They show that current models of radio-loud AGN evolution predict between 0.05 and 1 radio sources per square degree at $z > 6$ with $S_{150\text{MHz}} \geq 6$ mJy, adequate for EoR HI 21cm absorption studies with the SKA.

4 Observational challenges

4.1 Foregrounds

It has long been recognized that the HI 21cm signal from reionization must be detected on top of a much larger non-thermal (synchrotron) signal from foreground emission. This foreground includes discrete radio galaxies, and large scale emission from our own Galaxy. The expected HI signal is about 10^{-4} of the foreground emission.

Many groups have considered the effects of the foregrounds on HI 21cm EoR imaging and power spectral studies. (20) show that, even if point sources

can be removed to the level of $1 \mu\text{Jy}$, the rms fluctuations on spatial scales $\leq 10'$ ($l \geq 1000$) due to residual radio point sources will be $\geq 10 \text{ mK}$ just do to Poisson noise, increasing by a factor 100 if the sources are strongly clustered. Clearly this conclusion depends on the extrapolation of radio source populations to $\leq 1 \mu\text{Jy}$, but under reasonable assumptions, even in the Poisson case the residual source fluctuations will be comparable to the HI signal.

This calculation has led many groups to consider removal of foregrounds in the spectral domain. The important point is that the foregrounds should be relatively smooth in frequency, predominantly the sum of power-law, low frequency non-thermal spectra, or perhaps gently curving on spectral scales ≥ 10 's MHz. The HI signal should show significant structure on sub-MHz scales, corresponding to the typical size scale for features during reionization.

A number of complimentary approaches have been presented for foreground removal. (27; 68) consider removal of the foregrounds through fitting of smooth spectral models (power laws or low order polynomials in log space) to the observed visibilities or images. (46; 48) present a 3D Fourier analysis of the measured visibilities, where the third dimension is frequency. They show that the different symmetries in this 3D space for the signal arising from the noise-like HI emission, versus the smooth (in frequency) foreground emission, can be a powerful means of differentiating between foreground emission and the EoR line signal. (57; 6; 76) perform a similar analysis, only in the complementary Fourier space, meaning cross correlation of spectral channels. They show that the 21cm signal will effectively decorrelate for channel separations $> 1 \text{ MHz}$, while the foregrounds do not, and this too can be a means of separating the foregrounds from the desired 21cm fluctuations. The overall conclusion of these methods is that spectral decomposition should be adequate to separate non-thermal foregrounds from the HI 21cm signal from reionization at the mK level.

However, there are two potentially more insidious observational challenges relating to non-thermal foregrounds beyond simple in-beam confusion. First, there can be frequency dependent sidelobes from confusing sources in the very wide fields being considered. A particularly problematic effect has been the recent observation that telescope spectral response (ie. bandpass) may depend on position of a given source in the primary beam (54). The origin of this effect remains uncertain (perhaps relating to scattering and blocking structures), but it will lead to frequency dependent sidelobes that potentially affect widefields and are not removed through normal (on-axis) bandpass calibration, and may require a spatially dependent bandpass calibration.

And second is polarized structure in the diffuse emission in the field. Wide field polarization has been seen with low frequency observations with the WSRT at 330 MHz and below, and is thought to arise due to differential Faraday depth

through the ISM (31). Hence, great care is required to control, and calibrate, the wide field polarization response of the primary elements.

4.2 Ionosphere

A second potential challenge to low frequency imaging over wide fields is phase fluctuations caused by the ionosphere. These fluctuations are due to index of refraction fluctuations in the ionized plasma, and behave as $\Delta\phi \propto \nu^{-2}$. Moreover, the typical 'isoplanatic patch', or angle over which a single phase error applies, is a few to 10 degrees (physical scales of 10's km in the ionosphere), depending on frequency (17; 40). Fields larger than the isoplanatic patch will have multiple phase errors across the field, and hence cannot be corrected through standard (ie. single solution) phase self-calibration techniques.

New wide field self-calibration techniques, involving multiple phase solutions over the field, or a 'rubber screen' phase model (17; 32), are being developed that should allow for self-calibration over wide fields. However, even self-calibration techniques will be insufficient to overcome the very rapid variations caused by the occasional ionospheric storm, or traveling ionospheric disturbances.

At very low frequency (\leq a few MHz), one approaches the plasma frequency of the ionosphere, and the optical depth increases dramatically, precluding observations from the ground.

4.3 Interference

Perhaps the most difficult problem facing low frequency radio astronomy is terrestrial (man-made) interference. The relevant frequency range corresponds to 7 to 200 MHz ($z = 200$ to 6). These are not protected frequency bands, and commercial allocations include everything from broadcast radio and television, to fixed and mobile communications.

Many groups are pursuing methods for RFI mitigation and excision (see extensive references at (80)). These include: (i) using a reference horn, or one beam of a phased array, for constant monitoring of known, strong, RFI signals, (ii) conversely, arranging interferometric phases to produce a null at the position of the RFI source, and (iii) real-time RFI excision using advanced filtering techniques in time and frequency, of digitized signals both pre- and post-correlation. This requires very high dynamic range (many bit sampling), and very high frequency resolution.

One obvious advantage of HI absorption experiments (section 3.3) is that they can be done using long baselines (10's to 100's of km). Long baselines lead to decorrelation of the terrestrial signal due to fringe tracking of the celestial source. However, the fringe rates on the short baselines required for the HI emission experiments (\leq few km) are low, such that decorrelation due to fringe winding will not be a very effective RFI filter on the shorter baseline.

In the end, the most effective means of reducing interference is to go to the remotest sites. (85; 81) have selected sites in remote regions of Western Australia, and China, respectively, because of known low RFI environments. Of course, the ultimate location would be the back side of the moon.

5 Telescopes

Many programs have been initiated to study the HI 21cm signal from cosmic reionization, and beyond. These are summarized in Table 1. A number of different approaches are being taken, both technically and in order to address different aspects of the problem (48).

The largest near-term efforts are the Mileura Wide Field Array (MWA), the Primeval Structure Telescope (PAST), and the Low Frequency Array (LOFAR). These are being optimized to study the power spectrum of the HI 21cm fluctuations, although in principle they will be able to image the larger HII regions during reionization. The VLA-VHF system is designed specifically to set limits on the HII regions around $z \sim 6$ to 6.4 SDSS QSOs, although it should also constrain the late-time power spectrum. In the long term the Square Kilometer Array should have the sensitivity to perform true three dimensional imaging of the neutral IGM in the 21cm line during reionization. And at the lowest frequencies (< 50 MHz), the Long Wavelength Array (LWA), and eventually the lunar array (LUDAR (83; 84)), are being designed for the higher z signal, prior to reionization.

As discussed above, the technical challenges are many. Use of spectral decomposition to remove the foregrounds requires careful control of the synthesized beam as a function of frequency, with the optimal (although difficult) solution being a telescope design where the synthesized beam is invariant as a function of frequency (90). High dynamic range front ends are required to avoid saturation in cases of strong interference, while fine spectral sampling is required to avoid Gibbs ringing in the spectral response. The polarization response must be stable and well calibrated. Calibration in the presence of a significant ionospheric phase screen requires new wide field calibration techniques. The very high data rate expected for many element ($\geq 10^3$) arrays requires new methods for data transmission, cross correlation, and storage (85). At the low-

Table 1
HI 21cm Experiments

	Freq MHz	Area 10^4 m^2	B_{max} km	Site	Type	FoV deg	Date	Goal	Ref
GMRT	150 – 165	3.7	10	India	Parabola	4	2000	StromSph	(89)
PAST	50 – 200	7	2	China	Dipole	10	2006	PowSpec	(81)
VLA-VHF	180 – 200	1.3	1	USA	Parabola	4	2006	StromSph	(86)
Mark I	100 – 200		0	Aus	Spiral	180	2006	Global	(90)
MWA-LFD ¹	80 – 300	3	1.5	Aus	Dipole	20	2007	PowSpec	(85)
LOFAR ²	115 – 240	10	2km=40%	NL	Tiles	20	2007	PowSpec	(82)
LWA	10 – 88	10	5km=30%	USA	Dipole	20	2008	Pre-reion	(88)
SKA	100 – 200	100	5km=50%	?	Dipole	20	2015	Imaging	(87)
LUDAR	5 – 50	1000	100	Moon	Dipole	60	2020	pre-reion	(83)

¹An order of magnitude increase in area is planned after testing the Low Frequency Demonstrator.

²LOFAR will also have a low frequency component between 30 and 80 MHz.

est frequencies, $\leq 20\text{MHz}$ or so, where we hope to study the pre-reionization IGM, phase fluctuations and the opacity of the ionosphere becomes problematic, leading to the proposed LUDAR project on the far side of the moon. The far side of the moon is also the best location in order to completely avoid terrestrial interference.

Acknowledgements: Thanks to the Max-Planck Society and the Alexander von Humboldt Foundation for support through the Max-Planck Research Prize, and S. Furlanetto and N. Gnedin for permission to use figures.

References

- [1] Ali, Sk. 2005, MNRAS, in press, (astroph-0503237)
- [2] Barkana, R., Loeb, A. 2005, ApJ, 626, 1-11
- [3] Barkana, R., Loeb, A. 2005, ApJ, 624, L65-68
- [4] Barkana, R., Loeb, A. 2001, Phys. Rep. 349, 125-238
- [5] Bebbington, D. 1986, MNRAS, 218, 577-585
- [6] Bharadwaj, S. & Ali, Sk. 2005, MNRAS, 356, 1519-1428
- [7] Bowman, J, Morales, M., Hewitt, J. 2005, ApJ, in press (astroph-0507357)
- [8] Ciardi, B., Madau, P. 2003, ApJ, 596, 1-8
- [9] Ciardi, B., Stoehr, F., White, S. MNRAS, 343, 1101-1109
- [10] Carilli, C., Gnedin, N., Furlanetto, S., & Owen, F. 2004, NewAR, 48, 1053-1061
- [11] Carilli, C., Furlanetto, S., Briggs, F., Jarvis, M., Rawlings, S., Falcke, H. 2004, NewAR, 48, 1029-1038
- [12] Carilli, C., Gnedin, N., Owen, F. 2002, ApJ, 577, 22-30
- [13] Cen, R. 2003, ApJ, 591, 12-37
- [14] Chen, X. & Miralda-Escude, J. 2004, ApJ, 602, 1-11
- [15] Cooray, A. 2004, Phys. Rev. D, 70, 3509-3513

- [16] Cooray, A., Furlanetto, S. 2005, MNRAS, 395, L47-52
- [17] Cotton, W., Condon, J., Perley, R. et al. 2004, SPIE, 5489, 180-189
- [18] Davies, R., Pedlar, A., Mirabel, I. 1978, MNRAS, 182, 727-733
- [19] de Bruyn, A., Wieringa, M., Katgert, P., Sancisi, R. 1988, IAUS 130, 211-214
- [20] Di Matteo, T., Rosalba, P., Abel, T., Rees, M. 2002, MNRAS, 564, 576-580
- [21] Field, G.B. 1959, ApJ, 129, 551-565
- [22] Furlanetto, S. & Briggs, F. 2004, New AR, 48, 1039-1052
- [23] Furlanetto, S, Loeb, A. 2002, ApJ, 579, 1-9
- [24] Furlanetto, S., Zaldarriaga, M. Hernquist, L. 2004, ApJ, 613, 16-22
- [25] Furlanetto, S., Sokasian, A., Hernquist, L. 2004, MNRAS 347, 187-195
- [26] Furlanetto, S., McQuinn, D., Hernquist, L. 2005, ApJ, in press (astroph-0507524)
- [27] Gnedin, N. & Shaver, P. 2004, ApJ, 608, 611-621
- [28] Gnedin, N. 2004, ApJ, 610, 9-13
- [29] Gnedin, N. 2000, ApJ, 535, 530-554
- [30] Haiman, Z., Quartaert, E., Bower, G. 2004, ApJ, 612, 698-705
- [31] Haverkorn, M., Katgert, P., de Bruyn, A. 2004, A& A, 427, 549-559
- [32] Hopkins, P., Doeleman, S., Lonsdale, C. 2003, AAS, 203, 4005
- [33] Hirata, C.M. 2005, ApJ, in press (astroph-0507102)
- [34] Hogan, C., Rees, M. 1979, MNRAS, 188, 791-798
- [35] Hu, W. & Holder, G. Phys. Rev. D, 68, 3001-3004
- [36] Iliev, I., Scannapieco, E., Martel, H., Schapiro, P. 2003, MNRAS, 341, 81-90
- [37] Ioka, K. & Meszaros, P. 2005, ApJ 619, 684-696
- [38] Jarvis, M. & Rawlings, S. 2005, New AR, 48, 1173-1185
- [39] Kohler, K., Gnedin, N., Miralda-Escude, J., Shaver, P. 2005, ApJ, in press (astroph-0501086)
- [40] Lane, W., Cohen, A., Cotton, W., et al. 2004, SPIE, 5489, 354-361
- [41] Loeb, A., Barkana, R. 2001, ARAA, 39, 19-66
- [42] Loeb, A. & Zaldarriaga, M. 2004, Phys.Rev. Lett. 92, 1301-1304
- [43] Madau, P., Meiksin, A., Rees, M. 1997, ApJ, 475, 429-444
- [44] Meiksin, A. 2000, "Science with Large Antenna Arrays," (ASTRON: Netherlands), ed. M. van Haarlem p. 37-45
- [45] Miralda-Escude, J. 2003, Science, 300, 1904-1909
- [46] Mesinger, A., Haiman, Z. 2004, ApJ, 611, L69-72
- [47] Morales, M. & Hewitt, J. 2004, ApJ, 615, 7-18
- [48] Morales, M. 2005, ApJ, 619, 678-683
- [49] Nusser, A. 2005, MNRAS, 359, 183-190
- [50] Oh, S.P. & Furlanetto, S. 2005, ApJ, 620, L9-L12
- [51] Oh, S.P. & Haiman, Z. 2004, MNRAS, 346, 456-472
- [52] Oh, S.P. & Mack, K. 2003, MNRAS, 346, 871-877
- [53] Oort, M., Steemers, W., Windhorst, R. 1988, A & A Supp, 73, 103-123
- [54] Oosterloo, T. 2005, in *SKA Workshop, Wide Field Imaging*, (ASTRON:

- Netherlands), in press
- [55] Pritchard, J. & Furlanetto, S. 2005, MNRAS, in press (astroph-0508381)
 - [56] Salvaterra, R., Ciardi, B., Ferrara, A., Baccigalupi, C. 2005, MNRAS, 360, 1063-1068
 - [57] Santos, M., Cooray, A., Knox, L. 2005, ApJ, 625, 575-587
 - [58] Scott, D., Rees, M.J. 1990, MNRAS, 247, 510-516
 - [59] Sethi, S. 2005, MNRAS, in press (astroph-0508172)
 - [60] Shaver, P., Windhorst, R., Madau, P., de Bruyn A. 1999, A& A, 345, 380-390
 - [61] Sigurdson, B. & Cooray, A. 2005, ApJ, in press, astroph-0502549
 - [62] Spergel, D., Verde, L., Peiris, H. et al. ApJS, 148, 175-194
 - [63] Subrahmanyan, R., Kesteven, M., Ekers, R., Sinclair, M., Silk, J. 1998 MNRAS 298, 1189-1197
 - [64] Sunyaev, R., Zeldovich, Ya. 1972, A&A, 20, 189-200
 - [65] Tozzi, P., Madau, P., Meiksin, A., Rees, M. 2000, ApJ, 528, 597-606
 - [66] Uson, J., Bagri, D., Cornwell, T. 1991, Phys. Rev. Let, 67, 3328-3331
 - [67] Walter, F., Bertoldi, F., Carilli, C., et al. 2003, Nature, 424, 406-408
 - [68] Wang, X., Tegmark, M., Santos, M., Knox, L. 2005, ApJ, in press (astroph-0501081)
 - [69] White, R., Becker, R., Fan, X., Strauss, M. 2003, AJ, 126, 1-14
 - [70] Wouthuysen, S. 1952, AJ, 57, 31-33
 - [71] Wyithe, J.S., Loeb, A., Carilli, C. 2005, ApJ, 628, 575-582
 - [72] Wyithe, J.S., Loeb, A. 2004, Nature, 432, 194-196
 - [73] Wyithe, J.S., Loeb, A. 2004, ApJ, 610, 117
 - [74] Wyithe, J.S., Loeb, A., Barnes, D. 2005, ApJ, submitted, (astroph-0506045)
 - [75] Yu, Q. & Tremaine, S. 2002, MNRAS, 335, 965-976
 - [76] Zaldarigga, M., Furlanetto, S., Henquist, L. 2004, ApJ, 608, 622-635
 - [77] Zaldarigga, M., Furlanetto, S., Loeb, A. 2004, ??
 - [78] Zaroubi, S. & Silk, J. 2005, MNRAS, 360, L64 -67
 - [79] Zygelman, B. 2005, ApJ, 622, 1356-1362
 - [80] <http://www.atnf.csiro.au/SKA/intmit/>
 - [81] web.phys.cmu.edu/past/
 - [82] www.lofar.org/
 - [83] Corbin, M. et al. 2005, exploratory proposal to NASA
 - [84] Maccone, C. 2004, 35th COSPAR Assembly, p. 1415-1419
 - [85] web.haystack.mit.edu/arrays/MWA/LFD/index.html
 - [86] cfa-www.harvard.edu/dawn/
 - [87] www.skatelescope.org/
 - [88] lwa.unm.edu/index.shtml
 - [89] www.ncra.tifr.res.in/ncra_hpage/gmrt/gmrt.html
 - [90] Subrahmanyan, R., Chippendale, A., Ekers, R. 2005, ATNF newsletter, 56, 18-19